



Production and characterization of liquid crystal/polyacrylonitrile nano-fibers by electrospinning method

Atilla Eren Mamuk¹ · Çağdaş Koçak² · Çiğdem Elif Demirci Dönmez³

Received: 21 November 2020 / Revised: 17 April 2021 / Accepted: 17 April 2021

© The Author(s), under exclusive licence to Springer-Verlag GmbH Germany, part of Springer Nature 2021

Abstract

We present that high birefringent nematic liquid crystal, *4-n-pentyl-4'-cyanobiphenyl*, was incorporated into the polyacrylonitrile precursor which has a strong polar cyano group so as to produce electrospun nano-fibers, as the first time. Optical textures of nano-fibers were taken by polarized optical microscopy with different angles to determine the orientation degree of liquid crystal molecules in the center of the fiber. The molecules of liquid crystal self-ordered within the core of the fiber. Variation in morphology of liquid crystal/polymer nano-fibers were examined by utilizing both scanning electron microscopy and polarized optical microscopy depending on liquid crystal concentration in precursor and application voltage during electrospinning. Morphology of nano-fibers was significantly affected by electrospinning parameters and liquid crystal/polymer ratio. To understand phase separation and thermal stability of nano-fibers, calorimetric and thermogravimetric analyses were performed.

Keywords Liquid crystals · Polymer · Electrospinning · Nano-fiber · TGA · DSC · Globules in fiber

Introduction

Liquid crystals (LCs) are an important type of materials that exhibit anisotropic properties and give materials various physical properties. In addition to this, LCs have specific phase behavior which has both weak molecular ordering and rheologic properties likewise solid crystals and ordinary liquids, respectively [1]. This phase can be changed and controlled in different ways, such as surface interactions [2]. Despite liquid crystals that are generally researched in cell type samples for investigating optical properties and dynamics of defects [3, 4], they are quite suitable materials to be examined by combining them with various geometries and different types of materials. LCs may be prepared in much morphologies by merging with different materials such as azo dyes, polymers, and nano-

particles [5–7]. Thereby, various occasions/reasons arise to investigate the unique physical properties of LCs [8].

A great deal of work has been focused on improving thermal, optical, and structural properties of LCs by composing with polymers. LC/polymer composites are utilized in several applications such as artificial muscles [9], mirrorless lasing [10, 11], and a variety of flexible light-modulating devices [12–14]. In order to benefit some of the physical properties, such as anisotropy, self-ordering at the molecular level, and birefringence, LC/polymer composites are able to be formed in fiber. LCs have been produced in fiber structure as the core of a fiber by using different production techniques, for example, single-needle electrospinning, coaxial electrospinning, and airbrushing. The diameter of the fiber which is produced by electrospun and airbrushing is ordinarily less than 10 μm, thus limiting the diameter of the LC core to a couple of micron dimensions [15].

Recently, owing to generate microscale fibers with a core-sheath structure in which a liquid crystal or polymer core is encapsulated with a surrounding polymer shell, the electrospinning technique has been frequently used as a simple method [8, 16–19]. Reyes et al. [20] reported that electrospun mats of liquid crystal core fiber sensed the organic volatile vapors by responding to the optical changes. Also, electrospun LC/polymer fibers were reported as to have potential for some applications such that drug delivery, gas sensors,

✉ Atilla Eren Mamuk
aemamuk@mu.edu.tr

¹ Liquid Crystals Laboratory, Department of Physics, Muğla Sıtkı Koçman University, TR48000 Muğla, Turkey

² Molecular Nano-Materials Laboratory, Department of Physics, Muğla Sıtkı Koçman University, TR48000 Muğla, Turkey

³ The Center of Research Laboratories, Muğla Sıtkı Koçman University, TR48000 Muğla, Turkey

electronics [21–23], actuators in soft robotics and responsive textiles [10], and semi-flexible material [24]. Aside from electrospinning, it was reported that a solid polymer cylindrical core was separately submerged in both polymer and LC solutions as a new type of LC/polymer fiber production way, thus obtaining a three-layer cylindrical polymer/LC/polymer core-sheath structure fiber [15].

In this study, we showed that thermotropic LC/polymer core-sheath fibers are produced by single-needle electrospinning technique and how their optical, thermal, and structural properties change depending on LC/polymer ratio. Because of quite important benefits, polyacrylonitrile (PAN) was preferred for a polymeric host in our experiments: (i) that mean refractive index of PAN which is 1.53 at 25°C [25] is close to 1.60 at 23°C [26] of 5CB. Therefore, we expected transparent sheath to be achieved. (ii) PAN has polar cyano groups, in this way, it can influence and enhance some physical properties of LCs [27]. In previous studies, PAN was used several times with LCs or liquid crystalline materials for making a composite for altering the properties of LCs. Salim et al. [28] reported that PAN was used as a host in the precursor for producing liquid crystalline graphene oxide microfibers which were made by wet-spinning process. In [28], instead of LC, a quasi-liquid crystal material was used as a dopant, and microfibers were produced by using different methods from electrospinning. Chino et al. [29] reported that pure PAN was electrospun without mixing with any LC and collected over an ITO covered glass as a fiber mat and this deposited glass assembled with another glass as a type of sandwich cell; thereafter, LC was injected into the cell by capillary effect and was investigated under the influence of an electric field. Hence, LC/polymer structure has not been formed in [29]. In another study, some LCs and PAN were mixed to form a kind of polymer/gel structure, and the electro-optical properties of the structure were examined, but the fiber structure was not formed and/or focused [27]. In our research, the thermotropic nematic LC 5CB was incorporated into the core of PAN fibers by way of electrospinning in order to obtain nano-fiber for the first time. We successfully performed the self-assembly of the 5CB, which is widely used in researches and exhibits a liquid crystalline phase at room temperature, in the core of a nano-fiber by electrospinning process. Optical properties were given in order to determine the degree of birefringence of electrospun 5CB/PAN nano-fibers and these were related to the ability of the fibers to modulate light. Also, we performed structural characterization of nano-fibers to reveal the effects of electrospinning parameters and LC/polymer concentrations on the structure. Structural properties are pretty related to optical parameters of LC/polymer nano-fibers. In addition, thermal properties of nano-fibers were studied so as to determine how the 5CB concentration in composite affects the nematic-isotropic (N-I) phase transition temperature and to see the mass change of the nano-fiber

over time as the temperature changes. Depending on the results obtained, LC/polymer nano-fibers may be used in potential applications such as light-modulating devices and optical actuators or in different optical device applications.

Experimental

Materials

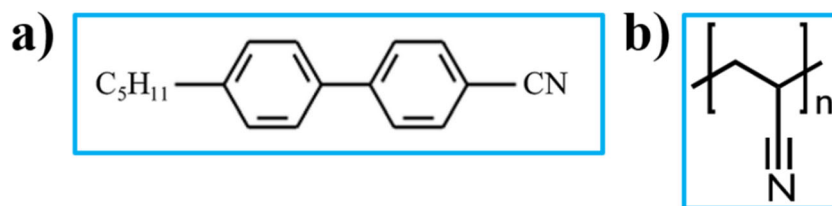
As a LC core, *4-n-pentyl-4'-cyanobiphenyl* (5CB) which was purchased from TCI Inc. was used as a LC. Scheme 1a demonstrates the molecular structure of 5CB. It shows nematic phase between 22 and 35°C temperature interval in the event of bulk state, and has a 0.18 birefringence at 23°C [30]. Phase transition temperatures may change depending on research conditions. The cyano group in the molecular structure of 5CB which can be regarded to be along the molecular long axis determines the dipolar moment and polarizability of its molecule [30, 31]. Therefore, 5CB is a compound of a high optical anisotropy and chemical stability in the nematic mesophase that makes it particularly favorable for LC/polymer structures.

Polyacrylonitrile (PAN) was used as an electrospinning host material and purchased from Sigma–Aldrich. The molecular weight of PAN is on average 150,000 *wt* (typical). PAN molecule consists of a strong nitrile group so it could serve polar structure and increase the interaction with other polar molecules. Since PAN becomes rigid into an amorphous state and shows a very low birefringence (≈ 0.01) [32], it can efficaciously be used as the sheath part of nano-fiber. Owing to be transparent in/ below micron-scale, PAN is quite suitable for LC/polymer fibers as a transparent sheath [27] in nanoscale. Dimethylformamide (DMF) is Reagent Plus grade, purchased from Sigma–Aldrich and used without further purification. DMF is as a strong polar solvent as so as to dissolve PAN.

Solution preparation

5CB/PAN precursors were prepared in five different concentrations, 8.88%, 19.17%, 42.86%, 49.91%, and 69.36%, and called M1, M2, M3, M4, and M5, respectively, and also tabulated in Table 1. Firstly, 7.6wt% PAN+DMF solution was prepared and 5CB/PAN precursors were prepared by adding the required amount of 5CB to the PAN+DMF solution in order to have 5CB/PAN ratios such as 8.88%, 19.17%, 42.86%, 49.91%, and 69.36%, and by stirring gently for a day—24 h. In each precursor, the 7.6wt% ratio was kept constant in PAN+DMF solution and it is used as a sixth precursor named M0.

Scheme 1 Chemical structure of (a) 5CB and (b) polyacrylonitrile (PAN)



Electrospinning system

PAN/5CB precursor was electrospun by using the Inovenso electrospinning device as depicted in Scheme 2. It is a compact device consisting of a programmable syringe pump with an accuracy of 0.001 ml/h, a 0.0–40.0 kV adjustable high voltage supply, and a needle target set up in a horizontal fashion; the needle is set as a positive pole and the target as a negative pole. The standard deep green syringe needle of 0.8 mm outer and 0.5 mm inner diameter was used as the needle throughout the experiments. After covering the metal target, a 20- μm -thick aluminum foil and glass substrates attached to the foil were used as a collector. The distance between the needle and collector, z , was set and kept at 23.0 cm for all electrospinning processes. The LC/polymer composite was collected under different electrospinning voltages that were 12.0, 15.0, 18.0, 21.0, and 24.0 kV and corresponding E-fields of 521.7, 652.2, 782.6, 913.0, and 1043.5 V/cm, respectively. During the collection, in order to obtain a fine-spinning jet, the flow rate of the precursor was adjusted from 0.15 to 3.00 ml/h depending on the concentration and the electrospinning voltage. All processes were performed at room temperature.

Polarized optical microscopy (POM)

Optical and morphological properties of pure PAN and LC/PAN nano-fibers were studied by using Olympus BX-51P polarized optical microscopy (POM) which is equipped with

optical retarders. In order to obtain textures of nano-fibers, firstly, samples of electrospun nano-fibers were collected over microscope slides; then, microphotographs of samples were taken by integrated Canon 6D camera between the crossed polarizers of POM in transmission mode.

Scanning electron microscopy (SEM)

The morphology and diameter of the nano-fibers were observed using an SEM (JEOL JSM-7600F; JEOL Ltd., Tokyo, Japan). All samples were sputtered for 60 s with a layer of gold under argon inert gas prior to SEM observation to get rid of charging effect and produce better quality images.

Differential scanning calorimetry (DSC)

DSC measurements were performed using a Perkin Elmer, DSC 8000 equipment to determine the temperature-dependent first-order phase transition characteristic of nano-fibers. Samples were sealed in aluminum pans. Empty aluminum pans with a weight of 0.02 mg were used as a reference for each measurement. Scanning rate of heating in the range of 30 to 50 $^{\circ}\text{C}$ was 5 $^{\circ}\text{C}/\text{min}$. Measurements were carried out under nitrogen gas with a flow rate of 20 ml/min. The mass temperature precision is stated as $\pm 0.008\%$ and the mass temperature accuracy is stated as $\pm 0.05\%$.

Scheme 2 A schematic drawing illustrating of single-needle electrospinning system

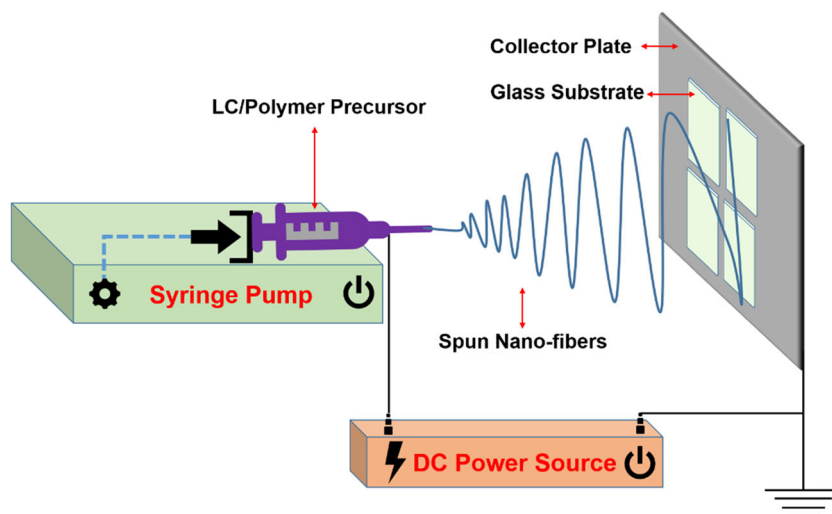


Table 1 The code of nano-fiber samples according to %5CB concentration in the precursor

The code of sample	% 5CB in precursor
M0	0
M1	8.88
M2	19.17
M3	42.86
M4	49.91
M5	69.36

Thermogravimetric analysis (TGA)

TGA was carried out using a Perkin Elmer, TGA 4000 equipment in the temperature range from 30 to 900 °C with a heating rate of 10 °C/min. Samples were placed in ceramic sample pans for the measurement. Measurements were carried out under nitrogen gas with a flow of 20 ml/min to determine the thermal properties of the nano-fibers. The initial masses used for measurement were determined as 5 mg for each sample. The mass measurement precision is stated as $\pm 0.01\%$.

Results

Optical properties of nano-fibers

According to our claim, we expected that LC within the nano-fiber solution should be self-settled inside electrospun nano-fiber as a cylindrical core and should be surrounded by polymer sheath. It has been reported in the literature that different techniques are used to determine whether there is LC in the fiber structure and whether the LC is oriented [12, 24, 33]. Lagerwall et al. [33] produced fibers in core-sheath structure by combining a liquid crystal with TiO₂ doped PVP polymer by coaxial electrospinning method. Polarized Raman spectroscopy was used to detect the presence and orientation of the liquid crystal within the fiber. The presence of peaks in Raman spectra of bulk LC at the same wavenumber as also observed in the LC/polymer fiber validated the existence of LC in the fiber structure [33]. As we indicated in “Materials,” 5CB shows high optical anisotropy and birefringence (0.18 at 23°C), whereas PAN shows very low birefringence (0.01 at 23°C). The existence of 5CB in fiber could be determined by considering the comparison of differences between the birefringence of PAN and 5CB. In order to prove our claim, we took textures of nano-fibers in various LC concentrations which were stayed between crossed polarizers with an additional 530-nm optical retarder and without any optical retarder under POM (Fig. 1). Textures of pure PAN fibers (M0) were also taken with the same method, as seen in Fig. 1. Textures in

Fig. 1 were obtained using POM in transmission mode with $\times 40$ magnification lens and with fixed incident light intensity. Depending on 5CB ratio in solution, birefringence changed. In Fig. 1a, the M0 nano-fibers are clearly observed by adding 530-nm retarder; however, they are not appearing under crossed polarizers since pure PAN does not exhibit birefringence (Fig. 1e). Figure 1b demonstrates that the M1 sample which has an 8.88% 5CB ratio has apparent electrospun nano-fibers by using optic retarder, but these nano-fibers shadowy appeared under crossed polarizers owing to having low LC concentration as seen in Fig. 1f. As the birefringence of PAN and 5CB is considered, it is quite normal that no birefringence could be observed for M0 at $\times 40$ magnification in comparison with the birefringence exhibited by M1 containing 8.88% liquid crystal. By increasing 5CB ratio from 8.88 to 69.36%, the brightening of nano-fibers noticeably increased because of high birefringence (Fig. 1e–h). With rising LC concentration, globules grew in size up. The reasons behind the formation of globules and their dependence on spinning parameters will be given in detail in “Morphological properties of nano-fibers.” Hereby, globules which are filled with LC are pretty visible under crossed polarizers (Fig. 1h). Additionally, with increasing the collection time of nano-fiber, the surface of the microscope slide was almost wholly covered by nano-fibers; thus, the samples which stayed between crossed polarizers appeared quite bright (SI 1). As a result, it is clear that LC/polymer homogeneity proceeded throughout the electrospinning process.

The brightness of a birefringent material oriented along a single direction depends on the angle between the crossed polarizers and the optical axis [34]. 5CB has positive birefringence and is uniaxial material. The polarization state of linearly polarized light coming to the LC, located in between crossed polarizer, changes after passing through LC and becomes elliptically polarized. Since elliptically polarized light has two components and only one component can pass through the analyzer, LC appears bright when observed by way of POM. The mathematical expression of the intensity of transmitting light from LC is given below:

$$I = I_0 \sin^2 2\varphi \sin^2 \frac{\delta}{2} \quad (1)$$

where I_0 , φ , and δ are the light intensity after the polarizer, the angle between the analyzer and the projection of the optical axis of LC molecules onto the sample plane, and phase difference between ordinary and extraordinary waves, respectively. The first sine term is substantially associated with the variation in the intensity of transmitting light [34]. In order to show the LC orientation in the fiber, one can perform an experiment which is birefringence as a function of the angle φ . In another approach, in Lagerwal’s study, it is proved that LC molecules settled along fiber direction by Raman spectra

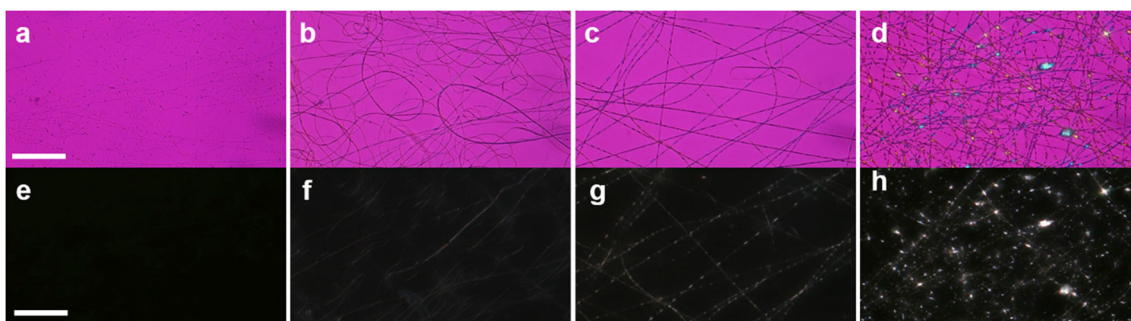


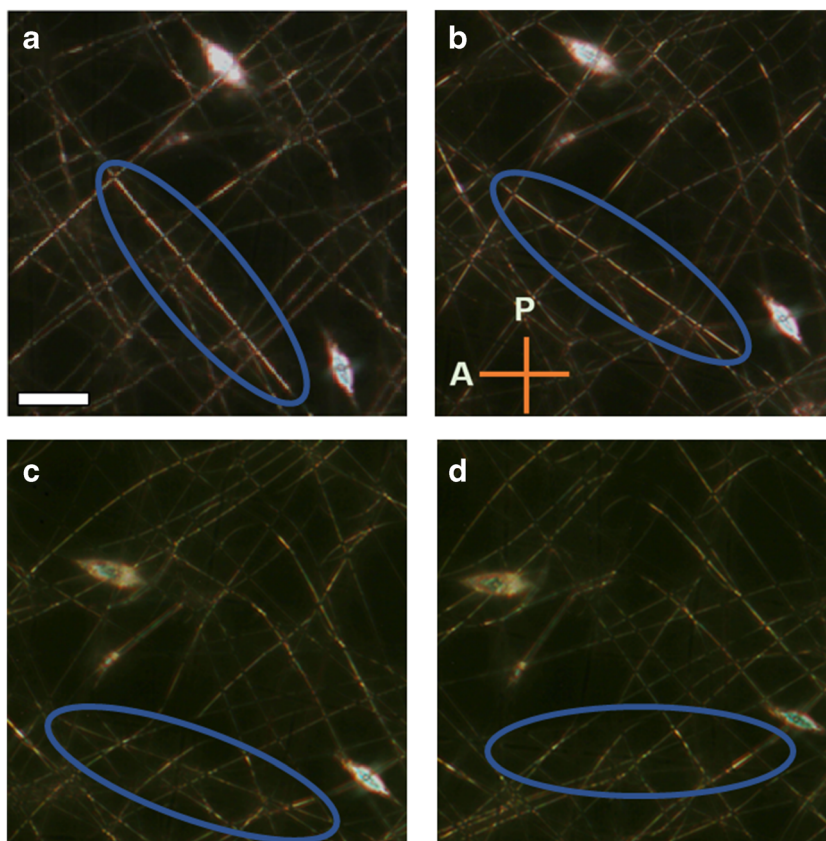
Fig. 1 POM images of nano-fibers collected on microscope glass are given in **a** to **d** between crossed polarizers with 530-nm optic retarder and **e** to **h** without retarder. **a** and **e** for sample M0 (pure PAN), **b** and **f** for sample M1, **c** and **g** for sample M3, and **d** and **h** for sample M5. All nano-

fibers were electrospun at 12.0-kV application voltage, 23.0-cm collection distance, one-minute collection duration. The scale bar represents 100 μm

obtained in different polarization directions [33]. In our study, when the LC sample is rotated around the angle φ of 45° and 0° with respect to the analyzer, the first sine term becomes maximum and minimum, i.e., the texture of LC appears brightest and darker, respectively. In Fig. 2a, some of the electrospun 5CB/PAN nano-fibers which are oriented 45° with crossed analyzer are observed pretty bright. By counter-clockwise rotating the sample, the brightness of oriented nano-fibers decreases (Fig. 2b–c) and finally nano-fibers seem completely dark coupled with fiber orientation parallel to the analyzer (Fig. 2d). It reveals that 5CB is planarly self-ordered within the core of PAN sheath because

of the great ordering strength affecting the spinning. The LC-polymer phase separation (core-sheath structure) in fibers spun by different generating technique was observed by Jakli's and West's research group [35–38]. In [35], the fibers were spun by single-needle electrospinning as we performed, and the change in the morphology of the fibers depending on relative humidity, solvent parameters, and production parameters was investigated. The proof of phase separation in fibers was demonstrated by POM analysis by utilizing the anisotropy properties of the LC [35]. In our study, temperature-dependent optical measurement was carried out to show that the core-sheath structure was formed. As is known, although

Fig. 2 Optical textures of M3 sample taken between crossed polarizer and analyzer are given in order to observe the variation of birefringence depending on the angle where LC molecules were oriented with respect to the analyzer. Textures were shot by rotating counter-clockwise at **a** 45° , **b** 30° , **c** 15° , and **d** 0° , with respect to the analyzer. The position of the polarizer and analyzer is given at **b**. Nano-fibers were spun at 24-kV application voltage, 23-cm collection distance, 1-min collection duration. The scale bar means 40 μm



LCs exhibit anisotropy within a certain temperature range, they behave like isotropic liquids above this temperature range [1]. In order to take advantage of the property of LCs, optical textures of the nano-fibers were taken below and above the N-I phase transition temperature (T_{NI}) between crossed polarizers. These temperature values are 28°C and 42°C, respectively. In Fig. 3, there are textures of M2, M4, and M5 samples taken at 42°C in the upper row. Nano-fibers with LC in the core do not appear in textures taken above the T_{NI} . Only in areas where the fibers are dense and thick are they very poorly visible due to the weak birefringence of PAN. In Fig. 3, in the lower row, there are textures of the same samples taken at 28°C. In these textures taken below the T_{NI} , the nano-fibers are clearly visible and shine under the cross-polarizer due to the high birefringence of the 5CB. This experiment, which was carried out by making use of the anisotropic behavior of the liquid crystal, also shows that the 5CB self-embedded in the fiber core. The mechanism of core-sheath formation may have occurred as follows: nematic LCs (such as 5CB that we used) are affected by external electric field [1]. Under high electric field, nematic LC molecules tend to align in the direction of the electric field. Considering this peculiarity, by inducing molecular orientation of LC under electric field during electrospinning, continuous LC/polymer nano-fibers through the electric field of electrospinning may be spun. In the electrospinning process, it is well known that the solvent evaporates very quickly in the high-speed electrospinning process with respect to fiber production with traditional drawing method. In this case, experimental studies reported in the literature show that there is not enough time for the molecular organization of liquid crystal molecules, and thus LC-polymer phase separation, revealed in core-sheath structure in our study, does not occur [39]. The DMF we used in our study has a low vapor pressure and the needle-collector distance was kept relatively high as $z = 23.0$ cm compared to

the distances reported in other studies [10, 40, 41]. Thus, either the solvent DMF did not evaporate rapidly or DMF had an enough travel time to move away from the structure by keeping the z distance wide, 23.0 cm. Therefore, 5CB LC might be oriented as a core inside the fiber due to the high elongational forces affecting the spinning jet. The optical birefringence study shown in Fig. 2 proved that the 5CB was arranged in planar orientation along the fiber. Yao et al. [42] reported that liquid crystal monomers (reactive mesogens) were oriented inside the fiber as a core in the core-sheath structure with the technique we used (single-needle electrospinning). Moreover, several interference colors which are incorporated by birefringence obviously appear within globules in Fig. 2. The second sine term in the Eq. 1 is responsible for these colors of the nano-fibers. It is the evidence of the existence of 5CB encapsulated by PAN.

Morphological properties of nano-fibers

In this part, we examined the morphological properties of 5CB/PAN nano-fibers depending on LC concentrations and applied voltages during the electrospinning process. Several factors, e.g., viscosity, surface tension, applied voltage, concentration of the solution, injection rate, and distance between the needle and collector, may affect the morphology of electrospun nano-fibers [39, 43]. We specified 5CB concentration in PAN and applied voltage as 8.88% - 19.17% - 42.86% - 49.91% - 69.36% by weight percentage and 12.0 kV - 15.0 kV - 18.0 kV - 21.0 kV - 24.0 kV, respectively. All samples were studied by using POM and SEM.

In Fig. 4, optical textures of samples in various concentrations captured between crossed polarizers and also by using 137-nm optical retarder are shown. During capturing textures in Fig. 4, although applied voltage and distance between collecting plate and electrospinning needle were kept fixed

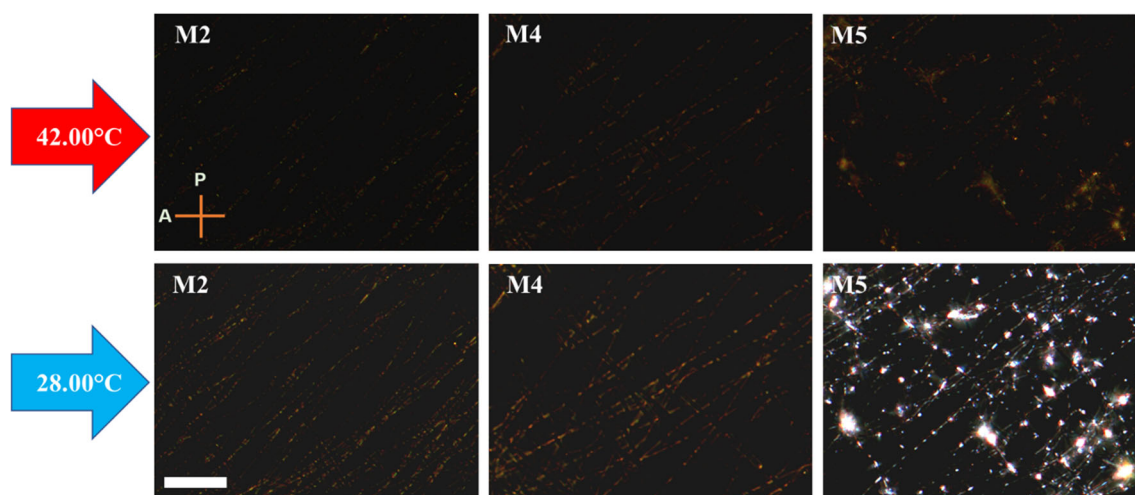


Fig. 3 Optical textures of M2, M3, and M5 samples taken between crossed polarizer and analyzer are given in order to observe the variation of birefringence depending on temperature. The scale bar means 60 μm

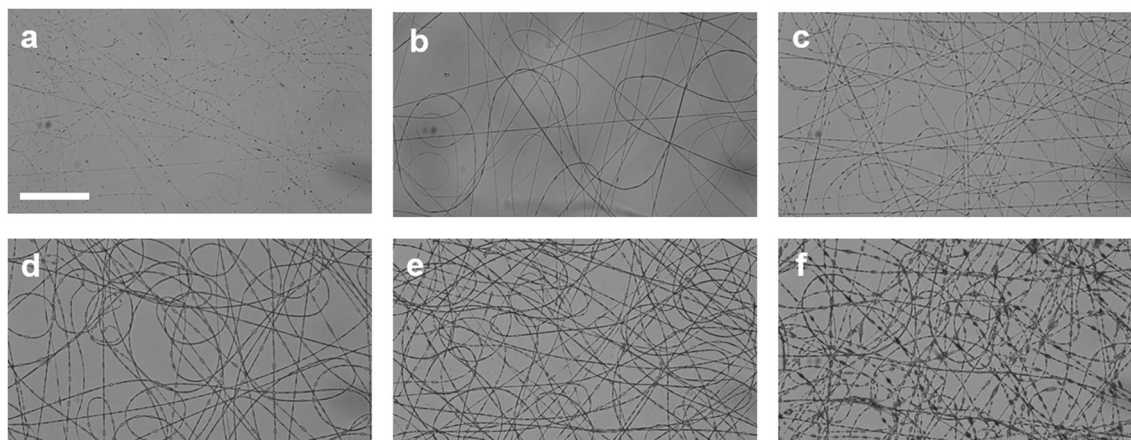


Fig. 4 Optical textures of M0 (pure PAN), M1, M2, M3, M4, and M5 are correlated with **a**, **b**, **c**, **d**, and **e**, respectively. Textures were taken by POM equipped with a 137-nm optical retarder, between crossed polarizers.

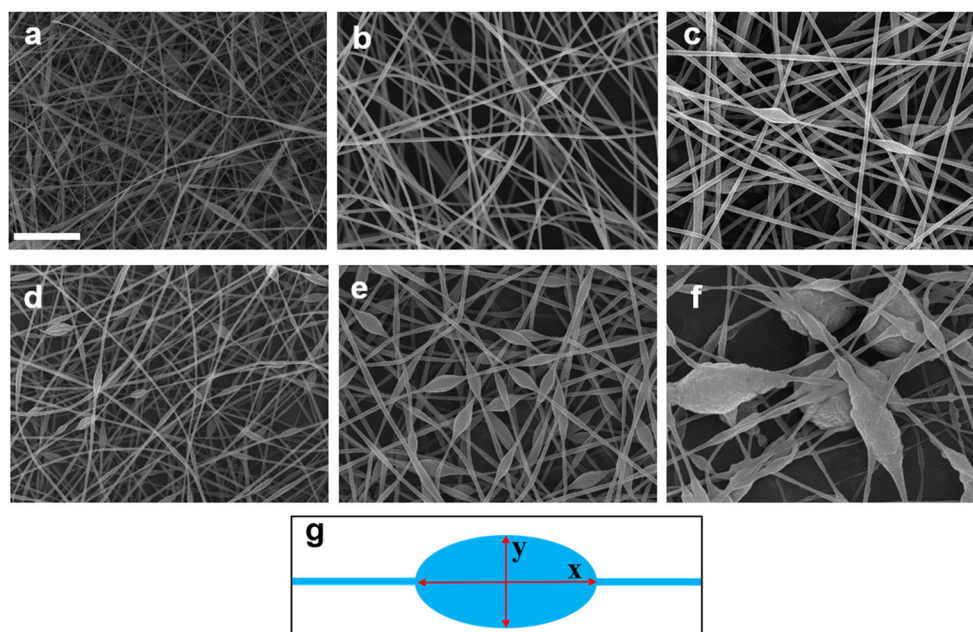
All samples were spun at 12-kV application voltage, 23-cm collection distance, and 1-min collection duration. The scale bar means 100 μm

12 kV and 23 cm, respectively, the injection rate of the LC/polymer solution was altered depending on the LC concentration in order to gain fine-spinning jet. The final fiber structure is strongly dependent on how fine is the spinning jet. The final fiber structure is highly dependent on the spinning quality and smoothness of the jet. What the quality and the smoothness meant is non-pulsed and dropletless jet, from Taylor cone, which we call a fine-spinning jet. Also, the collection time of nano-fibers was set to 1 min for each sample. Figure 4 shows that electrospun nano-fibers generated non-woven fiber mats with random fiber orientation. According to Fig. 4, the amount of electrospun nano-fiber per unit surface area increases relatively by raising 5CB concentration in structure. This result may be due to several reasons: as the ratio of 5CB in precursor increased, the viscosity of precursor decreased. The decrease in viscosity increased the spinning jet speed [39]. Moreover, regarding the decrease in viscosity, the increase in the injection rate caused the solution to exit the needle faster and the spinning jet speed to increase [44–46]. In our study, the injection rate was increased with the increase of 5CB in order to obtain a fine-spinning jet, as mentioned above. In addition, the viscosity decreased with the increase of 5CB in the precursor. For these reasons, it caused the solution to come out faster from the needle. Thus, in different precursors which had various 5CB concentration electrospun for the same time interval, the fiber density collected in the collector was also different. In addition, experimental results revealed that globules in different shapes existed along pure PAN and 5CB/PAN nano-fibers in various sizes. The electrospun nano-fibers exhibit discontinuities which are distributed relatively unsystematic; also, the 5CB is encapsulated in globules and in the 5CB/PAN nano-fiber cores. Despite very small globules that were determined at M1 (Fig. 4b), as the 5CB concentration increased, bigger globules were seen in the nano-fibers (Fig. 4c–f). By increasing the 5CB concentration, globules increase in size and the fiber morphology becomes non-uniform. At M5 sample which has the maximum LC ratio in structure, the LC globules

clustered too much and tear the polymer sheath in some regions, causing the structure to deteriorate (Fig. 4f). When the textures taken for different applied voltages were examined, similar results were indicated (SI 2). The authors thought that the increase in the size of globules by increasing 5CB concentration may be due to the decrease of precursor viscosity. In the literature, the formation of beading structures was also dependent on solution viscosity. In the studies conducted, as the viscosity decreased, while the application voltage and needle-collector distance was kept constant, it is concluded that the beading structures formed and grew [39, 44, 47]. In our study, the solution viscosity decreased as the 5CB ratio increased in the solution. In this context, globules were expected to increase regularly in size with the increase in 5CB concentration (resulting decrease in viscosity). In Figs. 4 and 5, it is clearly seen that the size of the beading structures increased.

In order to analyze the morphology of nano-fibers, SEM images were taken (Fig. 5a–f). Globules located along nano-fibers are clearly observed in both pure PAN nano-fibers and 5CB/PAN nano-fibers with various concentrations. Similar to the POM images, the size of globules was increased by increasing the 5CB concentration in the nano-fibers (Fig. 5). As we expected, in Fig. 5f which belongs to M5, the largest globules are clearly observed. In addition to this, entanglement between the nano-fibers and globules was specified in SEM image of M5 nano-fibers; thus, it supported the results of POM images. Besides, we studied on the mean value of thicknesses of nano-fibers and aspect ratio (AR) of globules at certain application voltage (12.0 kV) by using SEM images. AR is identified by calculating the width (y)/length (x) ratio depicted in Fig. 5g. Variation of nano-fiber thickness and AR of globules versus 5CB (%) in precursor are given in the same graph (Fig. 6). AR is a degree for being elongated of globules along the fiber from spherical to oval shape. Although M0 (pure PAN) shows smaller globules, it shows the relatively high AR. As soon as 5CB increases, AR of globules tends

Fig. 5 SEM images of M0 (pure PAN), M1, M2, M3, M4, and M5 are presented at **a**, **b**, **c**, **d**, **e**, respectively. All nano-fibers were spun at 12-kV application voltage, 23-cm collection distance, and 1-min collection duration. The scale bar means 5 μm . Also, the scheme of how aspect ratio is determined (AR) is shown in **g**



to decrease. Even though M1 nano-fibers show a slight decrease of its globules, M2 nano-fibers and M3 nano-fibers have minimum globules with AR. By maintaining 5CB concentration to rise, AR rapidly increases for relevant fibers and AR of M5 nano-fibers reaches almost the same value as the fiber of pure PAN. Moreover, the thickness of nano-fibers exhibits interesting variation depending on a 5CB% concentration in the structure. From M0 to M2, the thickness of nano-fiber properly increases an average from 160 to 320 nm. Then, thickness sharply decreases to an average of 170 nm in M3 nano-fibers; also, it is the minimum value among all LC/polymer samples. Afterwards, the thickness of nano-fibers properly rises again up to 330 nm in M5 nano-fibers which is the thickest, as a mean value. Regarding the variation of fiber thickness and AR of globules, these are linearly

proportional to increasing the injection rate with constant viscosity, application voltage, and needle-collector distance [44]. However, by keeping the application voltage, injection rate, and needle-collector distance constant, they would increase with the increase of viscosity of precursor [44, 45]. In our study, solution viscosity decreased with the addition of 5CB to the precursor. At the same time, in order to overcome such a handicap, the injection rate has been increased to obtain a fine-spinning jet with increasing 5CB in the precursor (i.e., decrease in viscosity). Both the decrease in the precursor viscosity (expected to decrease the fiber thickness) and increase in the injection rate (expected to increase the fiber thickness) to achieve a fine-spinning jet have been the main factors in the change of fiber thickness and AR of globules. Depending on the dominance of these two factors with each other, fiber thickness and AR may not show a regular change in Fig. 6.

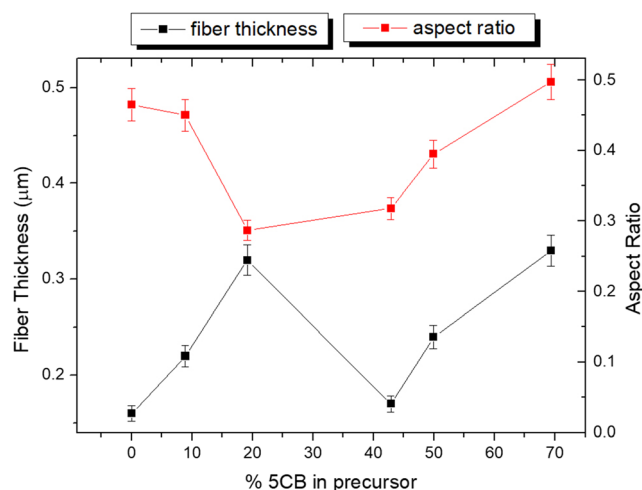


Fig. 6 Variation of nano-fiber thickness and aspect ratio (AR) vs 5CB ratio in the precursor is plotted

The effect of applied voltage on the morphology of the fibers was even studied. The applied voltage between conductive collector and needle during electrospinning is an important factor in order to get homogenous nano-fibers. By increasing voltage, it results in higher conductivity and fine spinning. The higher electrostatic driving force on the fluid jet helps the fiber to be thinner. This driving force is improved by increasing the applied voltage. In addition, if the applied voltage is increased further, the fiber solution leaves the needle more rapidly by spinning jet from the Taylor cone; thereby, it is expected that the thickness of nano-fiber increases [39]. In the literature, it has been determined both theoretically and experimentally that the globules form and are grown with the increase of the applied voltage for a sample whose concentration, viscosity, and needle-collector distance were kept constant [44–46]. In our study, it was determined that the globules increased with the increase in the application voltage.

Figure 7 shows the optical textures of the M5 sample that was taken under POM by adding a 530-nm retarder. Needle-collector distance was kept at 23.0 cm and applied voltage was varied from 12.0 to 24.0 kV by 3.0 kV step. The increase in application voltage gives rise to significant differences in the morphology of nano-fibers. There is a tentative change in globules of nano-fibers which produced under 12.0 kV and 15.0 kV (Fig. 7a–b). However, the size of globules obviously increases as the applied voltage continues to rise (Fig. 7c–e). The surface tension between the needle and the fluid forces the polymer solution to form droplets. However, the electrical and rheological forces impel the polymer solution to form fibers. The conflict between these two is responsible for the variance of globules' shape with increasing applied voltage [12, 45]. By analyzing the textures taken under 21.0 kV and 24.0 kV, it was identified that the size of the globules rose enough to cover neighbor nano-fibers and the nano-fibers became entangled/distorted in some regions (Fig. 7d–e). Furthermore, some globules tore due to disruption of sheath structure and regional LC-islands occurred. This case might be due to high electric field strength. We studied on mean values of AR of globules at a certain concentration depending on the application voltage by using POM images. The change in AR of globules for M0 nano-fibers and M3 nano-fibers is exhibited in Fig. 8. It was quite a different behavior in these two samples: although the regime of AR was not directly proportional for M0 (pure PAN) nano-fibers, it almost linearly increased for M3 nano-fibers. SI 3 which was taken under POM with 137-nm retarder supports the change in the size of both globules and aspect ratio depending on the applied voltage for sample M3.

Thermal properties of nano-fibers

Thermal analysis is an important part of the research in comprehension of a relation between the structure and property of polymer composite materials. Thermal analysis allows for

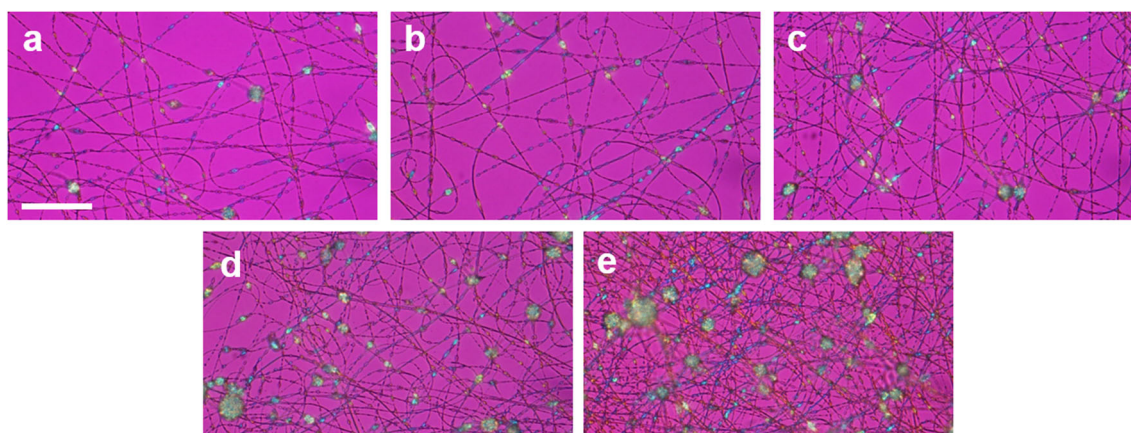


Fig. 7 POM images of nano-fibers which belong to M4 (49.91%) are given by using POM between crossed polarizers with equipped 530-nm optic retarder. All nano-fibers were spun at various application voltages

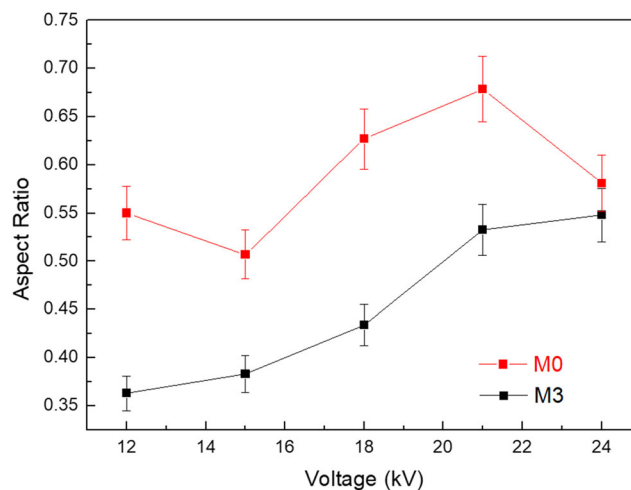


Fig. 8 Variation of and aspect ratio (AR) for M0 (pure PAN) and M3 (42.86%) vs application voltage is plotted

specifying the volatile compounds and the amount of humidity in polymeric materials. Also, the shifting of phase transition temperature of LC in fiber structure can be determined by performing thermal analysis of nano-fibers. In this sense, we performed thermogravimetric analysis (TGA) and differential scanning calorimetry (DSC) studies for nano-fibers and 5CB. Figure 9 shows TGA thermographs of both all nano-fiber samples and bulk 5CB LC. TGA gives us to study the weight loss and thermal deformation of samples. According to Fig. 9, there are three main stages of weight loss for all nano-fiber samples (not for bulk 5CB). In the first stage, a slender loss of mass was observed between 90 and 150°C for M0 nano-fiber (pure PAN). This weak decrease might be owing to leaving water which was due to humidity from the atmosphere [28, 40]. A similar case was revealed for other samples in the first stage. In the second stage, remarkable loss of mass which was resulted due to pyrolytic reactions took place from about 300 to 350°C, and the rest of the amount of mass was about 60%; also, it was possible that some volatile gases evolved in this

as **a** 12 kV, **b** 15 kV, **c** 18 kV, **d** 21 kV, and **e** 24 kV; 23-cm fixed collection distance, 1-min fixed collection duration. The scale bar means 100 μm

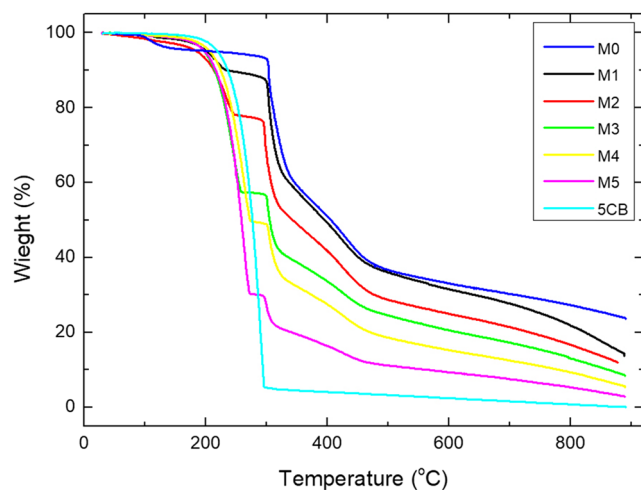


Fig. 9 TGA thermograph for all samples is plotted

period [48–50]. Further mass diminishing in the second stage was obviously indicated between 350 and 470°C for M0 and this loss might be correlated to the evaporating of NH_3 , HCN, or some other volatile products [28, 48, 51]. The third stage tediously took place at about 470 to 900°C which was the process limit; as a result, 25% char mass remained. Weight loss of 5CB depending on temperature increment was dramatically different from M0 (pure PAN). There was no important variation in loss of weight until about 200°C. After this point, variation of loss of weight in bulk 5CB sharply dropped to 5% of its total mass, as seen in Fig. 9. Then, total mass vanished slowly up to the exhaustion of whole mass. Considering the thermographs of 5CB and pure PAN (M0), by adding 5CB to the structure and increasing its amount, the loss in fiber mass increased from M0 to M5 in the same temperature interval. Although the beginning of the second stage of M1 was almost the same with M0, this initial temperature was negatively shifted from 295 to 245°C for M2 to M5, respectively. At the third stage, all nano-fibers monotonously lost their weight. As the amount of LC in the precursor increased, by considering the thermographs of 5CB and pure PAN (M0), the amount of residual mass expectedly decreased to about 14%, 11%, 9%, 6%, and 3% in the nano-fiber of M1, M2, M3, M4, and M5, respectively.

In order to determine the shift of N-I phase transition temperature, we studied on calorimetric measurement of nano-fibers and bulk 5CB. Short-range DSC temperature scan for M0, M3, M4, M5, and bulk 5CB is given in Fig. 10. DSC data of M1 and M2 are not given because there was no phase transition peak during scanning for mentioned samples. In the 5CB/PAN fibers, despite that it was explained in “Optical properties of nano-fibers” that almost all of the DMF used as a solvent left the fiber, a tiny amount of residual DMF (solvent) might exist in the fibers. The absence of N-I transition temperature peak in M1 and M2 might probably result from small quantities of the residual DMF that existed

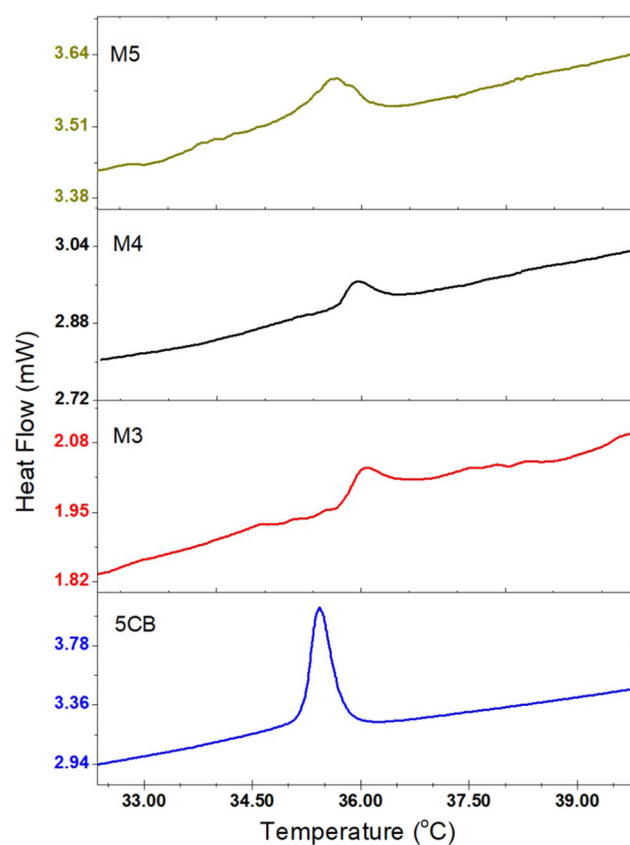


Fig. 10 Short-range DSC thermograph of M0 (pure PAN), M3 (42.86%), M4 (49.91%), M5 (69.36%), and also bulk 5CB is plotted. Due to any transition peak not observed, curves of M1 (8.88%) and M2 (19.17%) are not presented

in the nano-fiber. N-I phase transition temperature peak during heating process evidently revealed at 35.43°C for bulk 5CB. We did not detect any phase transition peak for the M0 sample; nevertheless, we gave the scanning data of M0 as a reference line. Relatively small transition peaks were found out for M3, M4, and M5 at 36.06°C, 35.96°C, and 35.63°C, respectively. It supports that 5CB might be completely phase-separated and self-ordered in the core of PAN sheath. By increasing 5CB in PAN precursor, N-I phase transition temperature almost linearly approached the transition temperature of bulk 5CB (Fig. 11). Lagerwall et al. [33] reported that N-I phase transition temperature shifted upper temperatures by a large number. The reason behind was evaluated as the change in composition of the precursor. The causes finding the transition temperature so high might be coaxial electrospinning technique and confinement of LC in the fiber core due to the technique. Another study by Buyuktanir et al. [12] stated no shift in transition temperature in the LC/polymer fiber which was electrospun with a similar technique as we used. The shifting on N-I phase transition temperature that we also observed was compatible with phase-separated polymer-dispersed liquid crystals (PDLC) which had high liquid crystal ratio in LC/polymer mixtures [52–54]. It has been thought that

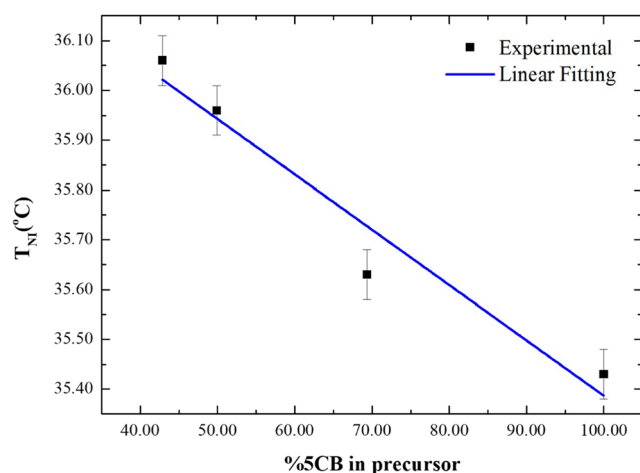


Fig. 11 Changing of N-I phase transition temperature

the very weak decrease in N-I phase transition temperature with the increase of 5CB ratio might be due to two different reasons. First, it is because of the growth of globules in the fiber structure. Second, it is because of the existence of a tiny amount of undesired residual solvent (impurity) in fibers. This undesired solvent which was DMF might suppress the N-I phase transition.

Conclusion

In this article, we generated 5CB/PAN composite nano-fibers as a core/sheath structure by using electrospinning technique and investigated optical, structural, and thermal properties of nano-fibers. We expected that 5CB should be self-settled inside electrospun nano-fiber as a core and that PAN should surround the 5CB as a polymer sheath after spinning. This expectation was proved by benefiting the anisotropic properties of 5CB under POM (Fig. 2). Also, taking advantage of the ability of liquid crystals that change the polarization direction of the incident light, we indicated that 5CB was planarly self-ordered within the core of PAN sheath. Considering the results in Fig. 2, 5CB/PAN nano-fibers may be a good candidate in potential applications such as light-modulating devices and optical actuators or in different optical device applications. Morphological properties of 5CB/PAN nano-fibers were studied depending on 5CB concentration and applied voltage. As a consequence of concentration-dependent analyses, optical textures taken by POM showed that oval-shaped globules existed along all nano-fibers and they increased in size by increasing the 5CB ratio in the precursor. Similar to the optical results of POM, the size of globules was increased by increasing 5CB concentration in the nano-fibers as seen in SEM images. Additionally, SEM images revealed that when the concentration increased almost above 50% nano-fibers and globules were entangled, so, electrospun nano-fiber became quite non-uniform. As regards to the shape of globules, i.e., aspect ratio, M2 and M3 nano-

fibers had the most elongated shape globules depending on LC ratio for 12-kV certain application voltage. In our study, very thin LC/PAN nano-fibers with 170–330 nm thickness were obtained statistically. The thickness of nano-fibers changed between almost 160 nm of M0 and 330 nm of M5. The statistically minimum thickness of LC/polymer was 170 nm which was observed in M3. Applied voltage crucially affected the morphology of nano-fibers; i.e., the size of globules obviously increased as the application voltage was raised. Eighteen-kilovolt application voltage may be regarded as threshold voltage in order to prevent the globules to get entangling and covering neighbor nano-fibers. Thermal analysis was performed and it gave quite important consequences. TGA results showed that the loss in fiber mass increased from M0 to M5 in the same temperature interval, by adding 5CB to the structure and increasing its amount. Moreover, since the existence of a tiny amount of undesired residual solvent in the fiber structure might suppress the N-I phase transition, N-I phase transition temperature weakly approached the transition temperature of bulk 5CB. Since the existence of the first-order N-I phase transition peak of 5CB was apparently observed starting from 42.86% LC/polymer ratio in DSC study, it is proved that 5CB could be exactly phase-separated in nano-fibers.

Supplementary Information The online version contains supplementary material available at <https://doi.org/10.1007/s00396-021-04842-5>.

Acknowledgements The authors would like to thank The Center of Research Laboratories, Mugla Sitki Kocman University and also Dr. Nejmettin AVCI for technical support.

Code availability Not applicable.

Author contributions A.E.M. designed research; A.E.M., Ç.K., and Ç.E.D.D. performed research and analyzed data; A.E.M. and Ç.K. wrote the paper.

Data availability The data that support the findings of this study are available from the corresponding author upon reasonable request.

Declarations

Conflict of interest The authors declare no competing interests.

References

- Demus D, Goodby J, Gray GW et al (1998) Handbook of liquid crystals. Wiley
- Dicker KT, Ratchford D, Casalini R, Thum MD, Wynne JH, Lundin JG (2020) Surfactant modulated phase transitions of liquid crystals confined in electrospun coaxial fibers. *Langmuir* 36:7916–7924. <https://doi.org/10.1021/acs.langmuir.0c01066>
- Özden P, Mamuk AE, Avci N (2019) Investigation of the viscoelastic properties of 4-propoxy-biphenyl-4-carbonitrile. *Liq Cryst* 46:2190–2200. <https://doi.org/10.1080/02678292.2019.1614236>

4. Zappone B, Mamuk AE, Gryn I, Arima V, Zizzari A, Bartolino R, Lacaze E, Petschek R (2020) Analogy between periodic patterns in thin smectic liquid crystal films and the intermediate state of superconductors. *Proc Natl Acad Sci U S A* 117:17643–17649. <https://doi.org/10.1073/pnas.2000849117>
5. Avci N, Hwang SJ (2017) Electrically tunable polarisation-independent blue-phase liquid crystal binary phase grating via phase-separated composite films. *Liq Cryst* 44:1559–1565. <https://doi.org/10.1080/02678292.2017.1303094>
6. Misra AK, Tripathi PK, Pandey KK, Pandey FP, Singh S, Singh A (2019) Electro-optic switching and memory effect in suspension of ferroelectric liquid crystal and iron oxide nanoparticles. *Mater Res Express* 6. <https://doi.org/10.1088/2053-1591/ab42c3>
7. Kiani S, Zakerhamidi MS, Tajalli H (2016) Hydrogen bonding intermolecular effect on electro-optical response of doped 6PCH nematic liquid crystal with some azo dyes. *Opt Mater (Amst)* 55: 121–129. <https://doi.org/10.1016/j.optmat.2016.03.019>
8. Liang HL, Enz E, Scalia G, Lagerwall J (2011) Liquid crystals in novel geometries prepared by microfluidics and electrospinning. *Mol Cryst Liq Cryst* 549:69–77. <https://doi.org/10.1080/15421406.2011.581140>
9. Li MH, Keller P, Antonietti M et al (2006) Artificial muscles based on liquid crystal elastomers. *Philos Trans R Soc A Math Phys Eng Sci* 364:2763–2777. <https://doi.org/10.1098/rsta.2006.1853>
10. Sharma A, Lagerwall JPF (2018) Electrospun composite liquid crystal elastomer fibers. *Materials (Basel)* 11:393. <https://doi.org/10.3390/ma11030393>
11. Finkelmann H, Kim ST, Muñoz A, Palffy-Muhoray P, Taheri B (2001) Tunable mirrorless lasing in cholesteric liquid crystalline elastomers. *Adv Mater* 13:1069–1072
12. Buyuktanir EA, Frey MW, West JL (2010) Self-assembled, optically responsive nematic liquid crystal/polymer core-shell fibers: formation and characterization. *Polymer (Guildf)* 51:4823–4830. <https://doi.org/10.1016/j.polymer.2010.08.011>
13. Büyüktanir EA, Gheorghiu N, West JL, Mitrokhin M, Holter B, Glushchenko A (2006) Field-induced polymer wall formation in a bistable smectic-a liquid crystal display. *Appl Phys Lett* 89:3–6. <https://doi.org/10.1063/1.2221887>
14. Stephenson SW, Johnson DM, Kilburn JI, Mi XD, Rankin CM, Capurso RG (2004) Development of a flexible electronic display using photographic technology. *SID Symp Dig Tech Pap* 35:774. <https://doi.org/10.1889/1.1821394>
15. Guan Y, Agra-Kooijman DM, Fu S, Jákli A, West JL (2019) Responsive liquid-crystal-clad fibers for advanced textiles and wearable sensors. *Adv Mater* 31:1–5. <https://doi.org/10.1002/adma.201902168>
16. Kim DK, Hwang M, Lagerwall JPF (2013) Liquid crystal functionalization of electrospun polymer fibers. *J Polym Sci B Polym Phys* 51:855–867. <https://doi.org/10.1002/polb.23285>
17. Enz E, Baumeister U, Lagerwall J (2009) Coaxial electrospinning of liquid crystal-containing poly(vinylpyrrolidone) microfibrils. *Beilstein J Org Chem* 5:1–8. <https://doi.org/10.3762/bjoc.5.58>
18. Enz E, Lagerwall J (2010) Electrospun microfibrils with temperature sensitive iridescence from encapsulated cholesteric liquid crystal. *J Mater Chem* 20:6866–6872. <https://doi.org/10.1039/c0jm01223h>
19. Kye Y, Kim C, Lagerwall J (2015) Multifunctional responsive fibers produced by dual liquid crystal core electrospinning. *J Mater Chem C* 3:8979–8985. <https://doi.org/10.1039/c5tc01707f>
20. Reyes CG, Sharma A, Lagerwall JPF (2016) Non-electronic gas sensors from electrospun mats of liquid crystal core fibres for detecting volatile organic compounds at room temperature. *Liq Cryst* 43:1986–2001. <https://doi.org/10.1080/02678292.2016.1212287>
21. Luzio A, Canesi EV, Bertarelli C, Caironi M (2014) Electrospun polymer fibers for electronic applications. *Materials (Basel)* 7:906–947. <https://doi.org/10.3390/ma7020906>
22. Han D, Steckl AJ (2013) Triaxial electrospun nanofiber membranes for controlled dual release of functional molecules. *ACS Appl Mater Interfaces* 5:8241–8245. <https://doi.org/10.1021/am402376c>
23. Xue J, Xie J, Liu W, Xia Y (2017) Electrospun nanofibers: new concepts, materials, and applications. *Acc Chem Res* 50:1976–1987. <https://doi.org/10.1021/acs.accounts.7b00218>
24. Bertocchi MJ, Ratchford DC, Casalini R, Wynne JH, Lundin JG (2018) Electrospun polymer fibers containing a liquid crystal core: insights into semiflexible confinement. *J Phys Chem C* 122:16964–16971. <https://doi.org/10.1021/acs.jpcc.8b04668>
25. Beevers RB (1964) Dependence of the glass transition temperature of polyacrylonitrile on molecular weight. *J Polym Sci A Gen Pap* 2: 5257–5265. <https://doi.org/10.1002/pol.1964.100021221>
26. Li J, Gauzia S, Wu S-T (2004) High temperature-gradient refractive index liquid crystals. *Opt Express* 12:2002–2010. <https://doi.org/10.1364/OPEX.12.002002>
27. Mashchenko VI, Goponenko AV, Udra CA, et al (2001) Use of polyacrylonitrile as promising material for matrix of liquid crystal composite. In: Belyaev VV, Kompanets in (eds) *Advanced display technologies: basic studies of problems in information display*. Proceedings of SPIE, Moscow, 4511, pp 127–132. <https://doi.org/10.1117/12.431273>
28. Salim NV, Jin X, Razal JM (2019) Polyacrylonitrile/liquid crystalline graphene oxide composite fibers – towards high performance carbon fiber precursors. *Compos Sci Technol* 182:107781. <https://doi.org/10.1016/j.compscitech.2019.107781>
29. Chino M, Kitano K, Tanaka K, Akiyama R (2008) Electro-optical properties of liquid crystal-polyacrylonitrile fibre composites. *Liq Cryst* 35:1225–1235. <https://doi.org/10.1080/02678290802509418>
30. Bogi A, Faetti S (2001) Elastic, dielectric and optical constants of 4'-pentyl-4-cyanobiphenyl. *Liq Cryst* 28:729–739. <https://doi.org/10.1080/02678290010021589>
31. Rozanski SA, Stannarius R, Groothues H, Kremer F (1996) Dielectric properties of the nematic liquid crystal 4-fi-pentyl-4'-cyanobiphenyl in porous membranes. *Liq Cryst* 20:59–66
32. An N, Xu Q, Xu L, Wu S (2006) Orientation structure and mechanical properties of polyacrylonitrile precursors. *Adv Mater Res* 11–12:383–386. <https://doi.org/10.4028/www.scientific.net/amr.11-12.383>
33. Lagerwall JPF, McCann JT, Formo E et al (2008) Coaxial electrospinning of microfibrils with liquid crystal in the core. *Chem Commun*:5420–5422. <https://doi.org/10.1039/b810450f>
34. Dierking I (2003) *Textures of liquid crystals*. Wiley
35. Wang J, Jákli A, West JL (2016) Morphology tuning of electrospun liquid crystal/polymer fibers. *ChemPhysChem* 17:3080–3085. <https://doi.org/10.1002/cphc.201600430>
36. West JL, Wang JR, Jákli A (2016) Airbrushed liquid crystal/polymer fibers for responsive textiles. *Adv Sci Technol* 100:43–49. <https://doi.org/10.4028/www.scientific.net/AST.100.43>
37. Wang J, Jákli A, West JL (2015) Airbrush formation of liquid crystal/polymer fibers. *ChemPhysChem* 16:1839–1841. <https://doi.org/10.1002/cphc.201500096>
38. Buyuktanir EA, West JL, Frey MW (2011) Optically responsive liquid crystal microfibrils for display and nondisplay applications. *Emerg Liq Cryst Technol VI* 7955:79550P. <https://doi.org/10.1117/12.880076>
39. Wu Y, An Q, Yin J, Hua T, Xie H, Li G, Tang H (2008) Liquid crystal fibers produced by using electrospinning technique. *Colloid Polym Sci* 286:897–905. <https://doi.org/10.1007/s00396-008-1845-7>
40. Zhang W, Wang Y, Sun C (2007) Characterization on oxidative stabilization of polyacrylonitrile nanofibers prepared by electrospinning. *J Polym Res* 14:467–474. <https://doi.org/10.1007/s10965-007-9130-x>
41. Enculescu M, Evangelidis A, Busuioic C et al (2014) Dependence on the dye's type and concentration of the emissive properties of

- electrospun dye-doped beaded nanofibers. *Dig J Nanomater Biostruct* 9:809–816
42. Yao J, Picot OT, Hughes-Brittain NF, Bastiaansen CWM, Peijs T (2016) Electrospinning of reactive mesogens. *Eur Polym J* 84:642–651. <https://doi.org/10.1016/j.eurpolymj.2016.08.037>
 43. Lin J-D, Chen C-P, Chen L-J, Chuang YC, Huang SY, Lee CR (2016) Morphological appearances and photo-controllable coloration of dye-doped cholesteric liquid crystal/polymer coaxial microfibers fabricated by coaxial electrospinning technique. *Opt Express* 24:3112–3126. <https://doi.org/10.1364/oe.24.003112>
 44. Cramariuc B, Cramariuc R, Scarlet R, Manea LR, Lupu IG, Cramariuc O (2013) Fiber diameter in electrospinning process. *J Electrostat* 71:189–198. <https://doi.org/10.1016/j.elstat.2012.12.018>
 45. Jacobs V, Anandjiwala RD, Maaza M (2010) The influence of electrospinning parameters on the structural morphology and diameter of electrospun nanofibers. *J Appl Polym Sci* 115:3130–3136. <https://doi.org/10.1002/app.31396>
 46. Haider A, Haider S, Kang IK (2018) A comprehensive review summarizing the effect of electrospinning parameters and potential applications of nanofibers in biomedical and biotechnology. *Arab J Chem* 11:1165–1188. <https://doi.org/10.1016/j.arabjc.2015.11.015>
 47. Okutan N, Terzi P, Altay F (2014) Affecting parameters on electrospinning process and characterization of electrospun gelatin nanofibers. *Food Hydrocoll* 39:19–26. <https://doi.org/10.1016/j.foodhyd.2013.12.022>
 48. Khan WS (2017) Chemical and thermal investigations of electrospun polyacrylonitrile nanofibers incorporated with various nanoscale inclusions. *J Therm Eng* 3:1375–1390. <https://doi.org/10.18186/journal-of-thermal-engineering.330180>
 49. Lee S, Kim J, Ku B-C, Kim J, Joh HI (2012) Structural evolution of polyacrylonitrile fibers in stabilization and carbonization. *Adv Chem Eng Sci* 02:275–282. <https://doi.org/10.4236/aces.2012.22032>
 50. Suzuki M, Wilkie CA (1995) The thermal degradation of acrylonitrile-butadiene-styrene terpolymer as studied by TGA/FTIR. *Polym Degrad Stab* 47:217–221. [https://doi.org/10.1016/0141-3910\(94\)00122-O](https://doi.org/10.1016/0141-3910(94)00122-O)
 51. Aslan S, Bal Altuntaş D, Koçak Ç, Kara Subaşat H (2020) Electrochemical evaluation of titanium (IV) oxide/polyacrylonitrile electrospun discharged battery coals as supercapacitor electrodes. *Electroanalysis* 33:120–128. <https://doi.org/10.1002/elan.202060239>
 52. Smith GW, Ventouris GM, West JL (1992) A calorimetric determination of fundamental properties of polymer-dispersed liquid crystals. *Mol Cryst Liq Cryst Sci Technol Sect A Mol Cryst Liq Cryst* 213:11–30. <https://doi.org/10.1080/10587259208028713>
 53. Smith GW (1990) Study of formation, phase behavior, and microdroplet size of a polyurethane-based polymer-dispersed liquid crystal. *Mol Cryst Liq Cryst Inc Nonlinear Opt* 180:201–222. <https://doi.org/10.1080/00268949008042203>
 54. Russell GM, Paterson BJA, Imrie CT, Heeks SK (1995) Thermal characterization of polymer-dispersed liquid crystals by differential scanning calorimetry. *Chem Mater* 7:2185–2189. <https://doi.org/10.1021/cm00059a029>

Publisher's note Springer Nature remains neutral with regard to jurisdictional claims in published maps and institutional affiliations.